Received: 10 July 2025 | Revised: 4 September 2025 | Accepted: 26 September 2025 | Published online: 17 October 2025

RESEARCH ARTICLE

Journal of Optics and Photonics Research
2025, Vol. 00(00) 1–8
DOI: 10.47852/bonviewJOPR52026746

BON VIEW PUBLISHING

Features of Restoration of Orientation of Nematic Liquid Crystals After Pulse Shift

Olga Denisova[1,*] and Yaroslava Abramishvili[2]

[1]Department of Physics, Ufa State Petroleum Technological University, Russia

[2]Institute of Educational Development, Bashkir State Medical University, Russia

Abstract: The aim is to study the processes of restoring the orientation of nematic liquid crystals (LCs) after a pulse shift. A sample of 4-octyl-4'-cyanobiphenyl was examined. The thickness of the LC layers ranged from 35 to 105 microns. The research methods included an experimental study of the effect of a mechanical shear pulse on thin layers of homeotropically oriented LCs (the Foner method) and theoretical modeling based on the Eriksen–Leslie equations. The experiment was carried out on a multilayer cell. Changes in the orientation of molecules were studied using optical imaging and recording of electrical signals. The obtained results showed a significant change in the temporal dynamics of light transmission and the angles of rotation of the director with a change in the amplitude and duration of the pulse. The main results showed that director relaxation occurs exponentially, and nonlinear effects such as the formation of domain structures and orientation waves were observed at amplitudes from 200 to 350 microns. At the same time, the relaxation time decreases rapidly. The proposed theory made it possible to explain the observed effects and calculate the relaxation time spectra. A satisfactory agreement was found between the theoretical and experimental relaxation time. The results obtained are important for improving the performance of LC-based devices such as displacement sensors, as well as understanding the fundamental mechanisms of the functioning of LC materials.

Keywords: nematic liquid crystal, orientation relaxation in liquid crystals, pulse shift

1. Introduction

Liquid crystals belong to a special group of substances that combine the characteristics of both the liquid state and solid bodies. The uniqueness of their physical and chemical characteristics determines broad prospects for practical application, covering such areas as the creation of screen panels, sensor elements, and biomedical devices. Of particular interest is the possibility of changing their structure and optical properties under the influence of external forces, such as an electric field, thermal action, or mechanical pressure.

Research on the problems of orientation instability of liquid crystals (LCs) under external influences is one of the most important areas of scientific research. Scientists are actively interested in this issue because understanding the nature of the appearance and evolution of orientation defects helps to improve the design and efficiency of devices based on LCs. The effect of a mechanical pulse on the homeotropic layer of a nematic liquid crystal (NLC) leads to a clarification of the preparation ("flash"). This phenomenon is called photoelasticity. The study by Han et al. [1] previously examined the influence of mechanical momentum and temperature on the manifestation of the photoelastic effect. It turned out that this effect is closely related to the features of the microstructure of the mesophase, the level of its organization, temperature, size, and nature of mechanical action. In another study by Arnous [2], an equation of NLC motion under the influence of a time-varying shear is presented. The authors show that two types of soliton solutions can exist, preserving their shape and moving at a speed directly related to the speed of shear application.

*Corresponding author: Olga Denisova, Department of Physics, Ufa State Petroleum Technological University, Russia. Email: physics_usptu@mail.ru

2. Literature Review

The phenomenon of orientation instability is caused by modifications in the orientation of LC molecules under the influence of external agents, among which mechanical stresses and electric fields are distinguished. Pulsed mechanical loads initiate specific manifestations of orientation instability, which are expressed in the formation of domain structures and regular configurations. Such effects have a significant impact on the temporal and spatial parameters of the propagation of light fluxes in LC media, which makes them the subject of close scientific interest. Detailed knowledge of the physical nature of these processes opens the way to creating highly effective methods for controlling the properties of LCs.

Scientific publications of previous years cover various aspects of the behavior of LCs under the influence of short-term mechanical loads. Thus, the study by Zhao et al. [3] suggests methods for monitoring the nucleation of domains in LCs under the influence of pulsed shear forces. Another scientific publication [4] focuses on the mechanisms of increasing the number of defects and their subsequent influence on the optical qualities of the material. Yun

© The Author(s) 2025. Published by BON VIEW PUBLISHING PTE. LTD. This is an open access article under the CC BY License (https://creativecommons.org/licenses/by/4.0/).

et al. [5] consider in detail the features of the viscoelastic behavior of LCs under sharp pressure jumps.

In addition, a separate area of research is focused on the analysis of topological mesh structures formed in LCs under the action of electric and magnetic fields. It was discovered that the number of vortex formations in such a network is regulated by the use of low-frequency electric fields, and a strong magnetic field can stabilize the position of the grid. The presented experimental facts are confirmed in the framework of a model based on the amplitude equation with corrections for inertial effects [6].

It was demonstrated in research by He et al. [7] that the use of polymer-stabilized cholesteric LCs makes it possible to create a bistable light barrier. By changing the concentration of polymer meshes, you can control the stability of both transparent and opaque phases. Optimization of the transmission spectrum is achieved by adjusting the spiral cholesterol pitch. The developed optical gateway is characterized by high energy efficiency, as it is able to maintain both stable configurations without external activation.

The influence of a pulsed magnetic field on the tribological characteristics of amorphous-nanocrystalline composites synthesized by high-speed plasma-powder sputtering is studied. The proposed pulse mode facilitates the high-speed plasma condensation procedure. The resulting coatings are characterized by a decrease in the level of porosity, the presence of laminar and sinusoidal magnetic domains, a significant content of amorphous and nanocrystalline structures, and improved tribological parameters compared to traditional coating technologies [8].

Functionalized LC “smart” windows controlled by sunlight are considered. Modern achievements in the development of LC windows with the introduction of functional dye compounds are described in detail, and the role of these dyes in the regulation of solar radiation and its application is emphasized. General design solutions and operating principles of LC windows containing functional components are presented. The mechanisms of dimming and converting the energy of sunlight in LC screens doped with dichroic, photosensitizing, and photothermal substances are noted. The current trends and potential advantages of LC windows that include these color additives are analyzed [9–11].

Szukalska et al. [12] and Xu et al. [13] are devoted to controlled generation based on the crystallization processes of a perylene dye introduced into the matrix of an NLC. Modern research in the field of optoelectronic technologies focuses on the development of laser systems that have a wide practical application. Of particular importance is the task of introducing laser television systems into the daily life of every consumer. In this study, a comprehensive analysis of the crystallization phenomenon in binary host-guest systems is performed using an LC matrix containing impurities. Special attention is paid to assessing the effect of different dye concentrations on the indicators of multicolored luminescence, laser efficiency, and morphology of the resulting material. The threshold energies of stochastic laser radiation are reviewed in detail, and the effect of constant potentials on the radiation intensity is analyzed. The ability to adjust the color gamut by varying the pump power indicates the great potential of such systems for future-generation laser displays.

In studies by Pagidi et al. [14] and Shivaraja et al. [15], an innovative device with a reduced operating voltage is proposed, implemented on the basis of nanostructured polymer dispersions of LCs containing ionic salts. The use of TFT technology has reduced the required control voltage by 40% by dispersing the ionic salt in the nano-structured polymer dispersed liquid crystals, while maintaining compatibility with existing standard devices. The technique provides a significant reduction in electrical intensity without deterioration of other electrophysical parameters, such as speed and contrast of the switched state. Results of measurements of frequency characteristics and response kinetics are published. The effect of reducing the required voltage is explained by the appearance of electrodynamic instability caused by local ion transfer near the LC-polymer interface, which weakens the retention of LC molecules and reduces the operating electric field strength. The model introduced by the authors provides a clear justification for the identified phenomenon of electric voltage drop.

Active colloidal particles in the LC medium were subjected to a thorough experimental study. In the absence of external force fields and the self-organizing motion of active particles, the Bose–Einstein condensate zones are in a passive state, and the equilibrium is characterized by the presence of a long-range orientation order. When an external electric field is applied, the active centers of the condensate begin to show activity, moving, rotating around themselves, interacting through mechanisms such as electrokinetic effects, Quincke rotation, and fixation on defects in the structure of the condensate. A system of tightly packed Quincke rotors located around spherical defects of the smectic structure demonstrates collective synchronous rotational motion with increasing degree of activity. Electrokinetic reactions in LCs proceed with acceleration proportional to the square of the electric field strength. The presence of an electric field creates a spatial charge as a result of optical distortions. Brownian motion in LCs exhibits both anisotropy and anomaly. The trajectories of movement of microorganisms are determined by the direction of the LC director. Living LCs exhibit bands with periodic instability and topologically chaotic turbulence. The macroscopic properties of LCs significantly determine the behavior of bacteria, in particular, the shape and trajectory of their movements. An increase in the density of bacterial cells and an increase in their activity lead to two consecutive stages of disruption of the orientation order of a living LC: initially, a stably directed director passes into a periodically curved structure, and a further increase in activity leads to the formation, decay, and mutual neutralization of pairs of positive and negative defects in dynamically changing topological chaos schemes. The properties of living LCs radically distinguish them from their corresponding isotropic analogues [16–18].

A new method for controlling the intensity of defect modes in multilayer photonic crystals equipped with an inner layer of an NLC is also proposed. Under the influence of an alternating electric field, various electrohydrodynamic domain structures (Williams domains, inclined rollers, and lattice forms) appear in the nematic layer. These domains cause polarization-sensitive light scattering effects, which lead to anisotropic suppression of the intensity of defect modes. By adjusting the applied voltage, it is possible to smoothly adjust the transmission rate of the photonic crystal spectrum, and this characteristic significantly depends on the direction of polarization of the incident light [19–23].

Despite significant progress in studying the orientation instability of LCs, important questions remain unresolved concerning the exact description of the processes of deformation and restoration of the structure of LCs after an external stimulus. This article is aimed at an in-depth study of the behavior of LCs when exposed to external fields. A comprehensive study of the effect of pulsed mechanical actions on thin layers of NLCs is carried out. Our approach includes a detailed consideration of the relationship between the parameters of mechanical shear and

Figure 1
Experimental cell with a liquid crystal (side view): 1 – conductive chromium Cr coating; 2 – glass plate; 3 – thin movable plate; 4 – gasket; 5 – liquid crystal

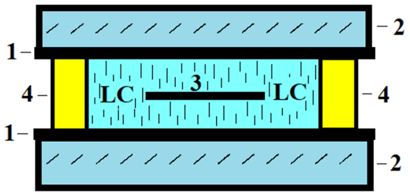

changes in the orientation of molecules, as well as identifying patterns that control the formation of domains and the restoration of the original structure. The results of our research allow us to better understand the nature of orientation instability and offer new possibilities for creating indicators for monitoring displacement, vibration, or pressure.

3. Materials and Methods

Thin layers of NLCs with a thickness h from 35 to 105 microns were studied. The orientation of the molecules was homeotropic. The object of study was 4-octyl-4'-cyanobiphenyl ($C_{18}H_{21}N$), which is found in the nematic phase in the temperature range 34.0–41.3 °C; it has a dipole moment of $p \sim 5.0\ D$ and a permittivity anisotropy of $\varepsilon_\alpha \approx 8.4$ [24].

For experimental studies of LC properties, sandwich cells were used (Figure 1). The cell was assembled from transparent glass plates (20 mm × 30 mm × 2 mm). A conductive chromium coating was applied to the plates, which provided a spontaneous homeotropic orientation of the LC molecules. A cover glass made in the form of narrow strips, measuring 5 mm × 20 mm and 130–200 microns thick (manufactured by Citotest), was placed as gaskets between the massive plates. To maintain the LC in the nematic phase, the cell was placed in a thermostat, the temperature of which was controlled by a thermocouple.

The Foner method was used to excite pulsed oscillations [25, 26]. Figure 2 shows a block diagram of the experimental setup. The cell was placed on the slide table of an optical microscope. The optical signal was recorded by voltmeters and a computer, and a video recording of the sample's behavior under external pulse action was also made. The main element of the recording part of the installation is the Amplival Pol U polarizing optical microscope and the SFN–10 spectrophotometric attachment. A coherent light source, the LGI-5 laser, was used for illumination. The wavelength of $\lambda = 627$ nm, corresponding to the wavelength of the laser radiation, was set on the scale of the SFN monochromator. The measurements were carried out with the polarizer and analyzer crossed. The light transmitted through the NLC cell, modulated by a change in the anisotropy of the refractive index of the medium, was converted into an electrical signal using a photomultiplier FEU-79. The light wave passing through the cell was recorded with a prefix of the SFN-10 type. The constant component of the luminous flux was then recorded by a DC millivoltmeter. The time-varying optical signal $I(t)$ was amplified and detected by a selective amplifier U2-8, and the signal was output to a recorder and computer. The selective amplifier U2-8 made it possible to register electrical signals in the range from 20 to 100 kHz. If it was necessary to simultaneously analyze and study the spectral composition of the studied signal, two paths were used, each of which independently allowed processing spectral harmonics. The measurements were carried out at an operating frequency of 120 Hz.

Figure 2
Block diagram of the installation for studying the pulse shift: 1 – a source of sound vibrations; 2 – a slide table; 3 – a polarizing microscope with a photometric attachment; 4 – a differential thermocouple; 5 – a DC microvoltmeter; 6 – a selective amplifier; 7 – an analog-to-digital converter (ADC); 8 – a computer; 9 – a device for measuring the pulse shift analysis of stationary ergodic random signals

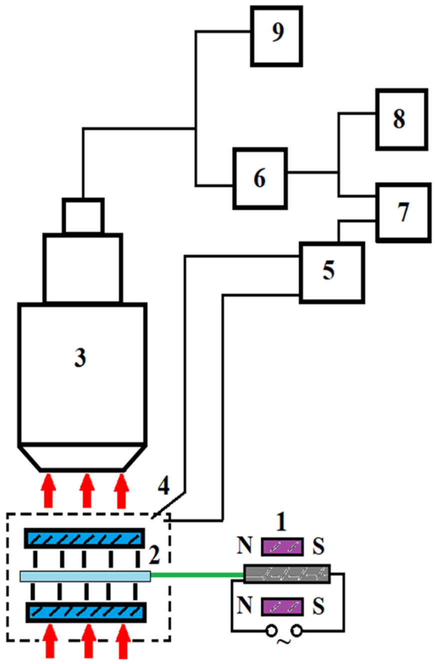

To create shear pulse disturbances in the NLC sample, the membrane of the source of mechanical vibrations was connected by a waveguide to a thin movable plate freely centered by tension forces in the LC volume (Figure 3). The amplitude of vibrations of the thin cell substrate was measured by inductive and optical methods. In the case of using the inductive method, the dependence of the oscillation amplitude of the movable plate on the voltage across the inductor was plotted. In the optical method, the amplitude was determined visually using a micrometer. The range of amplitudes under study is $a = 100$–600 microns.

Consider the effect of a pulse on a homeotropically oriented layer of nematic LC with a thickness of $h = 35$ microns. Omitting the intermediate calculations, we write out the equations of motion of the NLC for the velocity and formulate the initial and boundary conditions. For the chosen geometry, the equations of motion of the continuum of long axes and centers of inertia of molecules have the form [27], respectively:

$$K_{11}\frac{\partial^2 \delta n}{\partial y^2} + K_{33}\frac{\partial^2 \delta n}{\partial z^2} - \eta_4 \frac{\partial \delta n}{\partial t} + \eta_1 \frac{\partial \upsilon}{\partial z} = 0,$$

$$\rho \frac{\partial \upsilon}{\partial t} = \eta_o \frac{\partial^2 \upsilon}{\partial y^2} - \eta_1 \frac{\partial^2 \delta n}{\partial z \partial y} + \eta_3 \frac{\partial^2 \upsilon}{\partial z^2}, \quad (1)$$

where K_{ii} and η_i are the Frank elasticity and Leslie viscosity coefficients, n is the director of the LC, t is the time, y and z are the coordinates (z is directed perpendicular to the cell, and y is directed horizontally along the cell), and ρ is the density of the LC.

To simplify expressions, you should:

Figure 3
(a) Side view of the pulsed oscillation drive circuit and (b) top view: 1 – magnet; 2 – LC cell; 3 – coil; 4 – concentrator; 5 – waveguide; 6 – piezo emitters

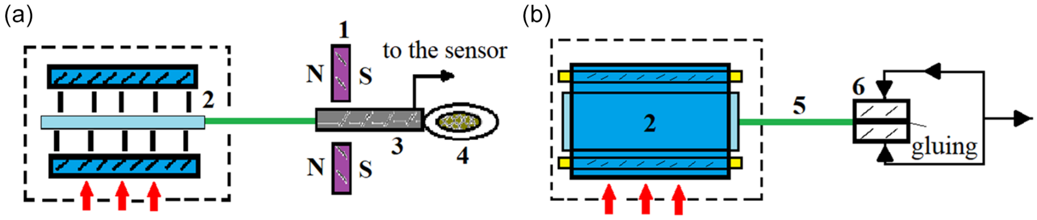

$$0,5(\alpha_4+\alpha_5-\alpha_2)=\eta_3$$

$$\eta_4=\alpha_3-\alpha_2=\gamma_1,$$

$$\eta_1=-\alpha_2,$$

$$\alpha_1+\alpha_2=\eta_o,$$

where $\alpha_4, \alpha_5,\ \alpha_2$ are the viscosity coefficients and γ_1 is the rotational viscosity.

In the following, we assume that the deviations of the director are small, that is, $\delta n \sim \theta << 1$.

We formulate the initial and boundary conditions for the director and velocities. Place the origin in the middle of the NLC layer. From the formulation of the problem for the angle of deviation of the director from the normal to the cell, it follows:

$$\theta|z=\pm d=0,\quad \theta|t=0=0, \tag{2}$$

where $\pm d$ are the coordinates of the surfaces of bounding NLCs.

Let's choose the perturbation in the general form, and then for the velocity, we write:

$$\upsilon|z=-d=f(y,t),\quad \upsilon|z=+d=0,\quad \upsilon|t=0=0. \tag{3}$$

Solving the problems (1–3) in a general form, even in a linear approximation, is very difficult. Therefore, we restrict ourselves to the case when the perturbation is only a function of time. In this case, the equations of motion have the form [27]:

$$\mathcal{K}_{33}\frac{\partial^2\theta}{\partial z^2}-\gamma_1\frac{\partial\theta}{\partial t}-\alpha_2\frac{\partial\upsilon}{\partial z}=0,$$

$$\rho\frac{\partial\upsilon}{\partial t}-\alpha_2\frac{\partial^2\upsilon}{\partial z\partial t}-\frac{1}{2}(\alpha_4-\alpha_5-\alpha_2)\frac{\partial^2\upsilon}{\partial z^2}=0. \tag{4}$$

Equation (4) under conditions (1–3) can be easily solved by the Laplace transform method [28]. In the image space, the expression for the velocity [27] is:

$$\bar{\upsilon}=F(p)\frac{\sin\lambda_2 d\ \ sh\lambda_1 z\ +\ sh\lambda_1 d\ \ \sin\lambda_2 z}{\sin\lambda_2 d\ \ sh\lambda_1 d},$$

where λ_1 and λ_2 *are* the roots of the characteristic equation of system (1) and *F(p)* is an image of the perturbation function *f(t)*.

The characteristic equation corresponding to the system of Equation (1) has the form [28]:

$$\frac{\eta_3}{\eta_4}\lambda^4+\frac{\eta_1^2-\rho\mathcal{K}_{33}-\eta_3\eta_4}{\mathcal{K}_{33}\eta_3}p\lambda^2+\frac{\rho p^2\eta_4}{\eta_3\mathcal{K}_{33}}=0.$$

In the case of pulsed perturbations considered in reference [28], the plate displacement can be represented as $y=y_o\delta(t)$, that is, $\upsilon|_{z=+d}=\upsilon_o\delta(t)$, when we have [27]:

$$\upsilon=\upsilon_o\sum_{n=0}^{\infty}\exp\left[-(2n+1)^2\frac{\pi^2}{4|\lambda_o^2|d^2}t\right]$$

$$\frac{\sin\lambda_2^{(n)}d\ \text{sh}\lambda_1^{(n)}z+\sin\lambda_2^{(n)}d\ \text{sh}\lambda_1^{(n)}d}{2\text{sh}(\lambda_1\pi/\lambda_o^2 d)(2n+1)^2}$$

$$\theta=\frac{\rho\upsilon_o}{\eta_1}\sum_{n=0}^{\infty}\exp\left[-(2n+1)^2\frac{\pi^2}{4|\lambda_o^2|d^2}t\right]\left[\text{sh}\lambda_2^{(n)}(2n+1)^2\left(\frac{\lambda_1^{(n)}\pi}{\lambda_o^2 d^2}\right)\right]^{-1}$$

$$\left[\left\{\frac{1}{\lambda_1^{(n)}\left(\sin\lambda_2^{(n)}d\ \text{ch}\lambda_1^{(n)}z-\sin\lambda_2^{(n)}d\ \text{ch}\lambda_1^{(n)}d\right)}\right.\right.$$

$$\left.-\frac{1}{\lambda_2^{(n)}(\text{ch}\lambda_1^{(n)}\ d\ \sin\lambda_2^{(n)}z-\text{ch}\lambda_1^{(n)}\ d\ \sin\lambda_2^{(n)}d\}}\right.$$

$$-\frac{\upsilon_o\eta_3}{\eta_1\left[\lambda_1^{(n)}\left(\sin\lambda_2^{(n)}d\ \text{ch}\lambda_1^{(n)}z-\sin\lambda_2^{(n)}d\ \text{ch}\lambda_1^{(n)}d\right)\right]}$$

$$\left.-\lambda_2^{(n)}\left(\text{ch}\lambda_1^{(n)}\ d\sin\lambda_2^{(n)}z-\text{ch}\lambda_1^{(n)}d\sin\lambda_2^{(n)}d\right)\right]\ \left[(2n+1)^2\frac{\pi^2 t}{4|\lambda_o^2 d^2|}\right], \tag{5}$$

where
$\lambda_o^2=-\frac{\alpha_2^2-\eta_3\gamma_1-\rho K_{33}}{K_{33}\eta_3}-\left[\left\{\frac{\alpha_2^2-\eta_3\gamma_1-\rho K_{33}}{K_{33}\eta_3}\right\}^2+\frac{\rho\gamma_1}{K_{33}\eta_3}\right]^{\frac{1}{2}};\ \lambda_{1,2}^{(n)}=\frac{\pi(2n+1)}{2d}$.

The value *of* λ_o^2 with a plus sign is discarded for physical reasons since it gives an increasing solution. Thus, in a linear approximation, it follows that the perturbation of the director relaxes according to the exponential law [27].

4. Results and Discussion

Let's consider an experimental situation. Figure 4(a) shows the shape of the shear pulse, and Figure 4(b) illustrates the relaxation dependence of amplitude on time. At relatively small pulse values (pulse duration t ≈ 0.065 s), the LC layer is uniformly illuminated, and the optical signal weakens to zero, which corresponds to the visible dark field in the microscope eyepiece.

The optical signal was recorded using an ADC. Next, the average square of the sine of the angle of deviation of the director from the normal was calculated, and its time dependences were

Figure 4
(a) Shape of the shear pulse; (b) relaxation dependence of amplitude on time

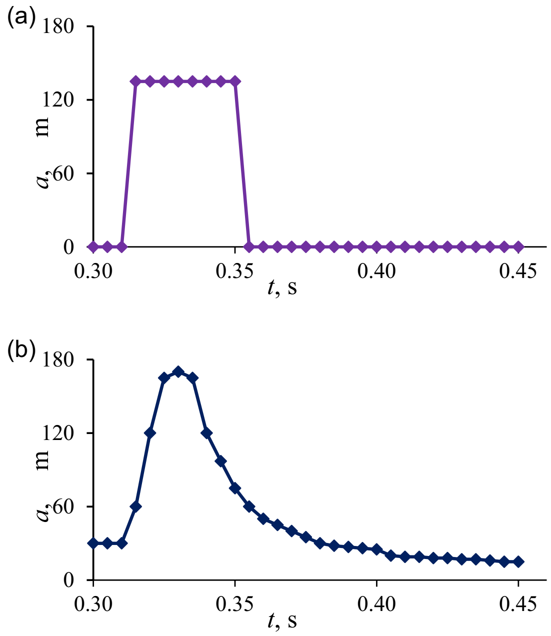

Figure 5
Relaxation dependences of (a) the intensity of the optical signal and (b) the mean square of the sine of a constant angle of inclination of the LC director

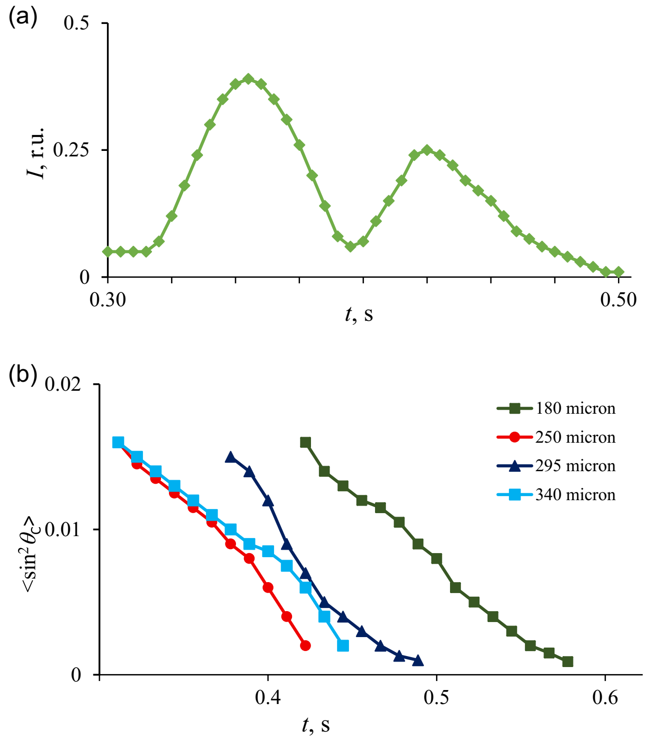

plotted for various pulse values (Figure 5(b)). Figure 5 shows the relaxation dependences of the relative I light transmission value at a pulse size $a \approx 250$ microns and the average square of the sine of the constant angle of inclination of the LC director $< \sin^2\theta_c >$ at different amplitudes of the pulse action ($a = 180, 250, 295, 340$ microns).

The presence of oscillations in the intensity of transmitted polarized light is associated with an optical phase $> \pi$ due to changes in the refractive index and relaxation processes of the director's reorientation to the initial homeotropic state. In this case, the dependence of the square of the average value of the sine of the angle of inclination of the director relative to the normal to the cell $< \sin^2\theta >$ on time is of great interest, where θ – is the angle of inclination of the director relative to the normal to the surface (Figure 5(b)).

Let us make quantitative estimates of the relaxation times τ_n, which follow from formula (5). Since

$$\tau_n = \frac{\tau_o}{(2n+1)^2},$$

where $\tau_o = \left(\frac{2\lambda_o d}{\pi}\right)^2$, then for the NLC layer with a half-thickness $d = h/2 = 1.75 \cdot 10^{-5}$ m, calculating the value $\tau_o \approx 1$ s.

The values of the material parameters are taken from the review [29]:

$K_{33} = 7.86 \cdot 10 - 12^{-12}$ N; $\eta_3 = 101.4 \cdot 10^{-3}$ N·s/m^3; $\gamma_1 = 72.8 \cdot 10^{-3}$ N·s/m^3; $\rho = 10^3$ kg/m^3;

$\alpha_2 = -77.0 \cdot 10^{-3}$ N·s/m^3; $\alpha_4 = 63.4 \cdot 10^{-3}$ N·s/m^3; $\alpha_5 = 62.4 \cdot 10^{-3}$ N·s/m^3.

Substituting the parameter values, we get the spectrum of times τ_n; for example, for $n = 1$, the calculated relaxation times are $\tau_o \approx 1$ s and $\tau_1 \approx 0.11$ s. Experimental values of the times are $\tau_o \approx 1.14$ s and $\tau_1 \approx 0.25$ s. We see that they are values of the same order, respectively.

The behavior of an NLC is usually described by the Eriksen–Leslie theory, which takes into account the influence of the first-order smallness velocity gradient. If the velocity gradient becomes large, then the theory stops working. In a real situation, with an increase in the shear rate, the viscosity of the nematic usually decreases, and the so-called shear "thinning" appears, so the strain relaxation rate is determined by two times from linear deformation and from shear "thinning." The latter is easily observed when, for example, in a lyotropic LC, the solution concentration increases, while in a thermotropic LC, the concentration decreases with increasing sample thickness since the order parameter depends on the thickness of the LC layer.

The coefficient for shifts of the "thinning" in this case [30] is:

$$k_c = 6D_r\left[\frac{9}{4}\left(\frac{c}{c^*} - \frac{8}{9}\right) + \frac{3}{4}\left(\frac{c}{c^*}\left(\frac{c}{c^*} - \frac{8}{9}\right)\right)^{1/2}\right]$$

where D_r is the rotational diffusion coefficient, c is the initial concentration in the isotropic state, and c^* is the volume concentration (in our case, $c^* = 1$).

Consider the viscoelasticity of a solution of rod-shaped molecules. The stress tensor of such a system consists of two terms: elastic stress and viscous stress. At small amplitudes of the action, the elastic stress does not affect the behavior of the LC. At large amplitudes of exposure, the viscosity of the LC decreases depending on the thickness of the sample.

De Gennes and Prost showed [24] that the dynamics of nematic particles is described fairly well by Landau's theory of phase transitions and proposed a phenomenological nonlinear equation for the tensor of the order parameter $S_{\alpha\beta}$:

$$\frac{\partial}{\partial t}S_{\alpha\beta} = F_{\alpha\beta}[S] + G_{\alpha\beta}[S],$$

where S is the order parameter and G is the Green's function (relaxation modulus of linear viscoelasticity):

Figure 6
Amplitude dependences: (a) relaxation times; (b) optical signal lifetime

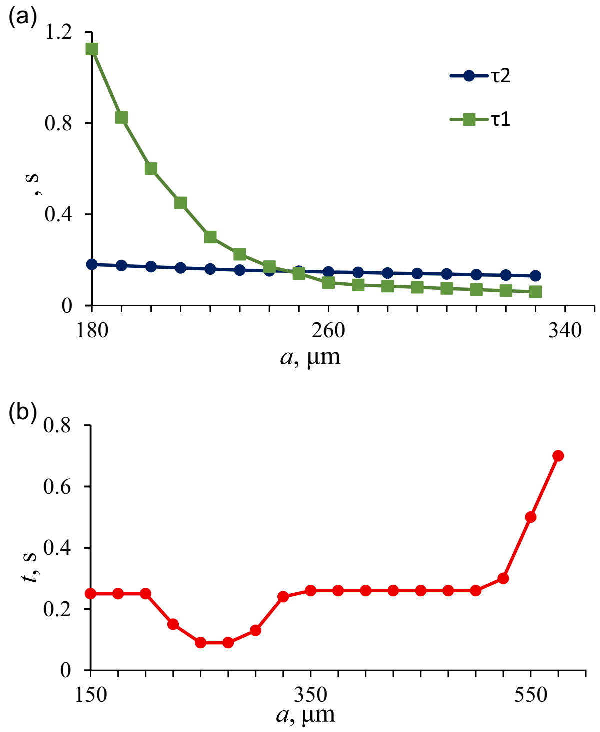

$$G_{\alpha\beta} = \frac{1}{3}\left(k_{\alpha\beta} + k_{\beta\alpha}\right) + k_{\alpha\mu}S_{\mu\beta} + k_{\beta\mu}S_{\mu\alpha} - \frac{2}{3}\delta_{\alpha\beta}k_{\mu\nu}S_{\mu\nu} - 2k_{\mu\nu}S_{\mu\nu}S_{\alpha\beta},$$

and the free energy of the Franc is:

$$F_{\alpha\beta} = -6\bar{D}r\left[\left(1 - \frac{U}{3}\right)S_{\alpha\beta} - U\left(S_{\beta\mu}S_{\beta\mu} - \frac{\delta_{\alpha\beta}}{3}S^2_{\mu\nu}\right) + US_{\alpha\beta}S^2_{\mu\nu}\right],$$

where $k_{\alpha\beta}$ is the strain rate tensor and $\delta_{\alpha\beta}$ is the Kronecker symbol, unit tensor (strain gradient).

The stress tensor is given as:

$$\sigma_{\alpha\beta} = 3\nu k_B T\left[S_{\alpha\beta}\left(1 - \frac{U}{3}\right) - U\left(S_{\alpha\mu}S_{\mu\beta} - \frac{1}{3}\delta_{\alpha\beta}S^2_{\mu\nu}\right) + US_{\alpha\beta}S_{\mu\nu}S_{\mu\nu}\right]$$

where U is the total interaction energy, k_B is the Boltzmann constant, ν is the amount of matter, and T is the temperature.

The dependences of the relaxation times τ and the existence of the optical signal t on the magnitude of the acting pulse a were constructed (Figure 6). Within the framework of the Eriksen–Leslie theory, the existence of two independent acoustic generation mechanisms is shown: convective and relaxation, which are characterized by two relaxation times τ_1 andτ_2. From the amplitude dependences, it follows that in the range of amplitudes from 200 to 350 microns, there is a decrease in the times τ (Figure 6(a)) and t (Figure 6(b)), which is associated with nonlinear processes occurring in the nematic layer [24, 30]. In addition, as predicted above by the Eriksen–Leslie theory, there are two relaxation times that are in good agreement with the theoretical values.

Visual analysis of the state of the nematic layer shows that at pulse magnitudes from 200 to 350 microns, the director relaxation character is fundamentally different from the state with a homogeneous deformation of the director field. In this case, the NLC layer is divided into linear domains orthogonal to the pulse direction with a period $d \approx 0.5$ mm. The further time dynamics of the resulting domains do not depend on the motion of the movable plate. In this case, the propagation of orientation waves occurs along and against the direction of the shear pulse so that orientation waves are formed, which, when their fronts interact, annihilate. In this situation, the relaxation time decreases dramatically. If the pulse value is increased further, the NLC illumination becomes homogeneous again, and orientation waves are not formed. The dependence $t(a)$ first reaches a plateau and then, at an amplitude value of 500 microns, begins to increase sharply, which is associated with large tilt angles of the director in the LC layer, orientation discontinuities – the director's flip at angles $\theta \geq \frac{\pi}{2}$.

5. Conclusion

In the course of these experiments, dynamic processes in thin layers of NLCs under the influence of pulsed mechanical influences were studied. The main attention was paid to the effect of the shear pulse on the orientation of LC molecules and subsequent relaxation phenomena. Under the influence of a mechanical impulse, the formation of spatial inhomogeneities is observed, with orientation waves propagating in the direction opposite to the applied force. It is established that the relaxation time of the nematic layer is inversely proportional to the square of the wavelength of displacements caused by a mechanical shock. This suggests that there are two time scales of the process: a fast relaxation period and a slow one due to the influence of the internal structure of the liquid. A comparative analysis of the theoretically calculated and experimentally measured values of relaxation times was performed, which showed a satisfactory agreement between the theory and experiment. Thus, the conducted research will allow us to better understand the physics of phenomena occurring in LCs under pulsed effects and increase the accuracy of modeling the behavior of LCs in real devices, which will improve the characteristics and devices based on them (e.g., pressure, displacement, vibration, and seismic activity sensors).

Ethical Statement

This study does not contain any studies with human or animal subjects performed by any of the authors.

Conflicts of Interest

The authors declare that they have no conflicts of interest to this work.

Data Availability Statement

Data are available from the corresponding author upon reasonable request.

Author Contribution Statement

Olga Denisova: Conceptualization, Methodology, Validation, Formal analysis, Investigation, Resources, Data curation, Writing – original draft, Writing – review & editing. **Yaroslava Abramishvili:** Formal analysis, Investigation, Writing – original draft, Visualization.

References

[1] Han, C.-Y., Chao, Z.-X., Chan, Y.-H., & Yu, C.-J. (2025). Programmable linear retarder using liquid crystal variable retarders with calibration for non-ideal beam splitter properties. *Optics and Lasers in Engineering*, *184*, 108623, https://doi.org/10.1016/j.optlaseng.2024.108623

[2] Arnous, A. H. (2025). Lie symmetries, stability, and chaotic dynamics of solitons in nematic liquid crystals with stochastic perturbation. *Chaos, Solitons & Fractals*, *199*, 116730. https://doi.org/10.1016/j.chaos.2025.116730

[3] Zhao, S., Chen, Y., & Huo, Y. (2023). Formation of lamellar domains in liquid crystal elastomers under compression. *International Journal of Mechanical Sciences*, *247*, 108185. https://doi.org/10.1016/j.ijmecsci.2023.108185

[4] Biçer, A., & Cicek, A. (2024). Liquid concentration sensing via weakly coupled point defects in a phononic crystal. *Journal of Molecular Liquids*, *409*, 125487. https://doi.org/10.1016/j.molliq.2024.125487

[5] Yun, H. S., Meijs, Z. C., Park, G., Fu, Y., Isa, L., & Yoon, D. K. (2023). Controlling liquid crystal boojum defects on fixed microparticle arrays via capillarity-assisted particles assembly. *Journal of Colloid and Interface Science*, *645*, 115–121. https://doi.org/10.1016/j.jcis.2023.04.100

[6] Clerc, M. G., & Gajardo-Pizarro, R. (2024). Nullclines entanglement induced topological transitions in driven liquid crystal cells. *Chaos, Solitons & Fractals*, *188*, 115447. https://doi.org/10.1016/j.chaos.2024.115447

[7] He, Z., Zeng, J., Zhu, S., Zhang, D., Ma, C., Zhang, C., . . . , & Miao, Z. (2023). A bistable light shutter based on polymer-stabilized cholesteric liquid crystals. *Optical Materials*, *136*, 113426. https://doi.org/10.1016/j.optmat.2022.113426

[8] Wang, Z., Huang, Y., Zhang, L., Zhou, J., Shan, D., Wang, H., & Xing, Z. (2022). Effect of a pulsed magnetic field on the tribological properties of amorphous/nanocrystalline composite coatings by supersonic plasma spraying. *Applied Surface Science*, *606*, 154853. https://doi.org/10.1016/j.apsusc.2022.154853

[9] Zhang, H., Guo, S., Miao, Z., & Shen, W. (2025). Functional dye-doped liquid crystal smart windows: From sunlight manipulation to sunlight utilization. *Sustainable Materials and Technologies*, *43*, e01244. https://doi.org/10.1016/j.susmat.2025.e01244

[10] Cao, S., Zhang, S., Zhang, T., Yao, Q., & Lee, J. Y. (2019). A visible light-near-infrared dual-band smart window with internal energy storage. *Joule*, *3*(4), 1152–1162. https://doi.org/10.1016/j.joule.2018.12.010

[11] Hemaida, A., Ghosh, A., Sundaram, S., & Mallick, T. K. (2021). Simulation study for a switchable adaptive polymer-dispersed liquid crystal smart window for two climate zones (Riyadh and London). *Energy and Buildings*, *251*, 111381. https://doi.org/10.1016/j.enbuild.2021.111381

[12] Szukalska, A., Zak, A., Chrzumnicka, E., Gibas, A., Baszczuk, A., & Mysliwiec, J. (2024). Crystallization-driven tunable lasing of perylene doped into the nematic liquid crystal. *Giant*, *18*, 100279. https://doi.org/10.1016/j.giant.2024.100279

[13] Xu, X., Sun, L., Shen, K., & Zhang, S. (2019). Organic and hybrid organic-inorganic flexible optoelectronics: Recent advances and perspectives. *Synthetic Metals*, *256*, 116137. https://doi.org/10.1016/j.synthmet.2019.116137

[14] Pagidi, S., Srivastava, A. K., Pandey, N., & Manda, R. (2024). Reduced driving electric field of ionic salt doped nano-structured polymer dispersed liquid crystals device. *Journal of Molecular Liquids*, *399*, 124444. https://doi.org/10.1016/j.molliq.2024.124444

[15] Shivaraja, S. J., Sahai, M., Gupta, R. K., & Manjuladevi, V. (2023). Superior electro-optical switching properties in polymer dispersed liquid crystals prepared with functionalized carbon nanotube nanocomposites of LC for switchable window applications. *Optical Materials*, *137*, 113546. https://doi.org/10.1016/j.optmat.2023.113546

[16] Lavrentovich, O. D. (2016). Active colloids in liquid crystals. *Current Opinion in Colloid & Interface Science*, *21*, 97–109. https://doi.org/10.1016/j.cocis.2015.11.008

[17] Degen, P. (2014). Self-propelling capsules as artificial micro swimmers. *Current Opinion in Colloid & Interface Science*, *19*(6), 611–619. https://doi.org/10.1016/j.cocis.2014.09.006

[18] Mushenheim, P. C., Trivedi, R. R., Weibel, D. B., & Abbott, N. L. (2014). Using liquid crystals to reveal how mechanical anisotropy changes interfacial behaviors of motile bacteria. *Biophysical Journal*, *107*(1), 255–265. https://doi.org/10.1016/j.bpj.2014.04.047

[19] Gunyakov, V. A., Krakhalev, M. N., Zyryanov, V. Y., Shabanov, V. F., & Loiko, V. A. (2016). Modulation of defect modes intensity by controlled light scattering in photonic crystal with liquid crystal domain structure. *Journal of Quantitative Spectroscopy and Radiative Transfer*, *178*, 152–157. https://doi.org/10.1016/j.jqsrt.2015.11.018

[20] Busch, K., von Freymann, G., Linden, S., Mingaleev, S. F., Tkeshelashvili, L., & Wegener, M. (2007). Periodic nanostructures for photonics. *Physics Reports*, *444*(3–6), 101–202. https://doi.org/10.1016/j.physrep.2007.02.011

[21] Shan, Y., Krishnakumar, A., Qin, Z., & Mao, H. (2022). Reducing lateral stair-stepping defects in liquid crystal display-based vat photopolymerization by defocusing the image pattern. *Additive Manufacturing*, *52*, 102653, https://doi.org/10.1016/j.addma.2022.102653

[22] Gao, Y., Yan, W., Gao, T., Chen, Q., Yang, W., Xie, Q., . . . , & Li, L. (2020). Properties of the structural defects during SiC-crystal-induced crystallization on the solid-liquid interface. *Materials Science in Semiconductor Processing*, *116*, 105155. https://doi.org/10.1016/j.mssp.2020.105155

[23] MacDonald, C. S., Mackenzie, J. A., & Ramage, A. (2020). A moving mesh method for modelling defects in nematic liquid crystals. *Journal of Computational Physics: X*, *8*, 100065. https://doi.org/10.1016/j.jcpx.2020.100065

[24] de Gennes, P. G., & Prost, J. (1993). *The physics of liquid crystals* (2nd ed.). UK: Oxford University Press. https://doi.org/10.1093/oso/9780198520245.001.0001

[25] Denisova, O. (2022). Liquid crystal lambda-probe for car. *Transportation Research Procedia*, *63*, 244–253. https://doi.org/10.1016/j.trpro.2022.06.010

[26] Denisova, O. (2022). Molecular relaxation in a liquid crystal after switching off the acoustic action. In *XIV International Scientific Conference "INTERAGROMASH 2021": Precision Agriculture and Agricultural Machinery Industry, Volume 2*, 51–60. https://doi.org/10.1007/978-3-030-80946-1_6

[27] Sai, D. V., Yoon, T. H., & Dhara, S. (2020). Studies on binary mixtures of nematic liquid crystals made of strongly polar molecules with identical cores and antagonistic orientation of permanent dipoles. *Journal of Molecular Liquids*, *312*, 113410, https://doi.org/10.1016/j.molliq.2020.113410

[28] Visakh, P. M., Semkin, A., & Özdemir, Z. G. (Eds.). (2022). *Liquid crystal polymer nanocomposites*. UK: Woodhead Publishing. https://doi.org/10.1016/B978-0-12-822128-0.09991-X

[29] Emsley, J. W. (2025). The structure and orientational order of molecules in nematic liquid crystal phases. *Progress in Nuclear Magnetic Resonance Spectroscopy.* Advance online publication. https://doi.org/10.1016/j.pnmrs.2025.101576

[30] Buka, Á., & Éber, N. (2018). Nematic liquid crystals: Instabilities. In *Reference module in materials science and materials engineering*. Elsevier. https://doi.org/10.1016/B978-0-12-803581-8.11265-2

How to Cite: Denisova, O., & Abramishvili, Y. (2025). Features of Restoration of Orientation of Nematic Liquid Crystals After Pulse Shift. *Journal of Optics and Photonics Research*. https://doi.org/10.47852/bonviewJOPR52026746